Seawater Debye Model Function at L-band and Its Impact on Salinity Retrieval from Aquarius Satellite Data

Yiwen Zhou, *Member*, *IEEE*, Roger H. Lang, *Fellow*, *IEEE*,
Emmanuel Dinnat, *Senior Member*, *IEEE*, and David M. Le Vine, *Fellow*, *IEEE*

***Abstract* — A model function of seawater, which specifies the dielectric constant of seawater as a function of salinity, temperature and frequency, is important for the retrieval of sea surface salinity using satellite data. In 2017, a model function has been developed based on measurement data at 1.4134 GHz using a third-order polynomial expression in salinity (*S*) and temperature (*T*). Although the model showed improvements in salinity retrieval, it had an inconsistent behavior between partitioned salinities. To improve the stability of model, new dielectric measurements of seawater have been made recently over a broad range of salinities and temperatures to expand the dataset used for developing the model function. The structure of the model function has been changed from a polynomial expansion in *S* and *T* to a physics-based model consisting of a Debye molecular resonance term plus a conductivity term. Each unknown parameter is expressed in *S* and *T* based on the expanded measurement dataset. Physical arguments have been used to limit the number of unknown coefficients in these expressions to improve the stability of model function. The new model function has been employed in the retrieval algorithm of Aquarius satellite mission to obtain a global salinity map. The retrieved salinity using different model function is compared with in-situ data collected by Argo floats to evaluate the impact and the performance of model functions. The results indicate that the new model function has significant improvements in salinity retrieval compared with other existing models.**

***Index Terms* — seawater, Debye model, Aquarius, sea surface salinity retrieval, satellite data**

I. Introduction

SEA surface salinity (SSS) has important meaning for understanding the global water cycle, ocean currents and circulation. L-band Earth-observing satellites have been employed to sense SSS remotely, e.g. Soil Moisture and Ocean Salinity (SMOS) [1], Aquarius/SAC-D [2][3] and Soil Moisture Active Passive (SMAP) [4]. These satellites operate inside the frequency band at 1.400 – 1.427 GHz, which is protected from man-made radio emissions for passive use only. The satellite's instrument measures the brightness temperature (T_b) of the emission from the sea surface to retrieve the SSS. In order to retrieve salinity from the observed ocean brightness temperature, an expression is needed for the dielectric constant of seawater as a function of salinity (S) and physical temperature (T) [5]. This expression is called the model function $\varepsilon(S,T)$.

The model function for the dielectric constant of seawater can be developed by fitting a function to the measurement data. It is difficult to measure the seawater dielectric constant since seawater can corrode the device and undermine the repeatability of measurements [6]. Over the years, there have been a few dielectric measurements of seawater made at microwave frequencies [6]-[11]. In particular, the measurements of Ho et al. [8] and Blanch and Aguasca [11] have been made at L-band. These measurements are summarized in [12]. For L-band measurements, Ho et al. [8] employed a reflection cavity technique to determine the seawater dielectric constant. Their measurements, however, may have had errors for high values of salinity and temperature due to a heating effect [6] since the cavity reflection technique needs more power to operate than a transmission-type cavity. Blanch and Aguasca [11] used a transmission cell method but their results have not been reported in the refereed literature.

A common approach valid for developing the model function of seawater is to employ a Debye model for the resonance of the water molecule plus a conductivity term [13]. This model structure will be referred to as the Debye form for convenience in this paper. Most of the existing model functions, e.g. Stogryn [6][13], Klein and Swift [14], Ellison [10] and Meissner and Wentz [15]-[17], have a single Debye form (for low frequency) or a double Debye form (for low and high frequencies); these models are summarized in [18]. Differences exist between these L-band model functions [12]. These literatures, in addition, don't always provide a complete analysis of how the Debye parameters are derived from experimental data. Of the several model functions referred to above, the Klein and Swift [14] (hereinafter KS) and Meissner and Wentz [15]-[17] (hereinafter MW) model functions are the most widely used. These two models will be compared with the new model function introduced in this paper.

The George Washington University (GW) developed a seawater dielectric model function in 2017 [18], which will be referred to as the GW2017 model, based on the lab

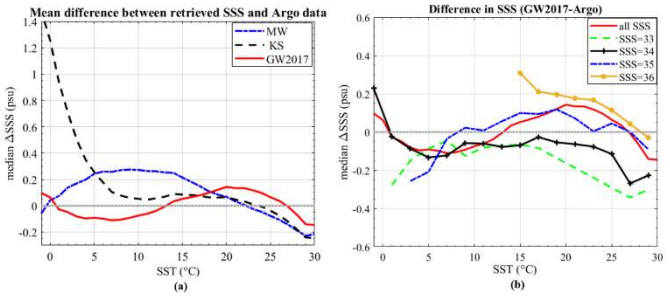

Fig. 1 (a) Difference between the salinity retrieved from Aquarius observation and in-situ salinity (Argo data) using three model functions for the dielectric constant: Klein-Swift (KS), Meissner-Wentz (MW) and GW2017. Aquarius observations have been recalibrated for each model function; (b) Results of (a) for the GW2017 model function are shown for different values of salinity.

measurement data reported in [12]. The GW2017 model function has been developed by expanding the dielectric constant in a third-order polynomial in S and T; the coefficients are then evaluated from measurement data. The GW2017 model function has been used in the Aquarius satellite inversion algorithm to determine the SSS from the Aquarius data collected from 2011 to 2015 [18]. The differences between these retrieved values and the in-situ data collected by Argo floats are shown in Fig. 1 (a) where the results are averaged over Sea Surface Salinity (SSS) and plotted as a function of Sea Surface Temperature (SST). The same procedure was applied to the KS and MW model functions and their performance is also shown in Fig. 1 (a). It is seen that the averaged SSS retrieved by using GW2017 model function is closer to Argo data when compared with the other two model functions.

Further investigations have been made to examine the performance of GW2017 model function. It has been found that although the GW2017 model has very small fitting errors, the system matrix for solving the polynomial coefficients has a large condition number. It indicates that the inversion is close to ill-conditioned and the model is very sensitive to the noise and fluctuation in the data. The SSS retrieved by the GW2017 model, as a result, show dispersions when compared with in-situ data for different salinities. Fig. 1 (b) shows the dispersion in the difference between the retrieved salinity and Argo data for individual salinities. The dispersion can cause relatively large SSS-dependent errors in the global SSS map. This behavior is not observed when using the KS or MW model functions even though the GW2017 model function has a better performance on average when considering all salinities.

In this paper, a new model function is proposed with a Debye form instead of the third-order polynomial. The Debye model of seawater has three parameters that can be expressed as polynomials in S and T. The coefficients of these polynomials need to be evaluated based on the measurement data. In finding the coefficients of these parameters, the condition is imposed that the dielectric constant of seawater must reduce to the dielectric constant of distilled water as the salinity approaches zero. This constraint has the effect of reducing the number of unknown coefficients that are required for each of the three Debye unknown parameters. Terms in the expansions that do not follow trends in the experimental data are eliminated. The condition number in each of the three inversions, as a result, is significantly reduced. The resulting model is less sensitive to the noise in the data, which results in a more stable performance with less dispersion in salinity retrieval.

In order to implement the above inversion procedure, dielectric measurements of distilled water have been made from 0ºC to 35ºC with a 5ºC interval. More measurements have been made for seawater with 10, 20, 34 and 36 psu from 0ºC to 30ºC with a 5ºC interval to improve the model and expand its domain of applicability. In addition, measurements for seawater with salinity 30, 34 and 35 psu and temperatures from -1.5ºC to 3ºC have been made to further investigate the dielectric constant of seawater at low temperatures.

This paper is structured as follows: Section II introduces the new dielectric measurements made since 2018. Section III provides a detailed procedure of developing the Debye model function based on the measurement data. In addition, the comparison of the new model function and other existing models is presented. In Section IV, the application of the new model function in salinity retrieval is discussed. The SSS global map is obtained for different model functions; the difference between the retrieved salinity and in-situ data is demonstrated. Finally, the conclusion is presented in Section V.

II. New Seawater Measurements

Measurements of the seawater dielectric constant have been made during past years for developing a dielectric model function [12]. A naval brass microwave cavity is used to measure the complex dielectric constant of seawater at 1.4134 GHz. The seawater is introduced into the cavity through a capillary glass tube, which has an inner diameter of 0.1 mm. After the seawater sample is introduced, it perturbs the field inside the cavity causing a change in both the resonant frequency and the cavity quality factor, Q (i.e. the resonant frequency divided by the bandwidth). The real and imaginary parts of the seawater dielectric constant are determined by the changes in the resonant frequency and Q, respectively, before and after the sample is introduced. Before 2018, seawater dielectric measurements have been made at salinity values of 30, 33, 35, 38 psu from 0°C to 35°C with a 5°C interval between temperatures. The detailed measurement procedures and results have been reported in [12]. Note that when the temperature changes, the size of cavity slightly expands or shrinks accordingly. This expansion/shrinkage causes a slight change in the resonant frequency of cavity. The cavity resonates from 1.4128 to 1.4140 GHz at temperature ranging from 35°C to 0°C, respectively. In this paper, the averaged frequency, 1.4134 GHz, is employed in the model development. The error caused by this approximation is lower than 0.035% with the greatest error occurring at 35° C.

Based on the in-situ data from the Argo network of freely drifting floats, it is found that most open ocean salinity measurements clustered from 34 to 36 psu (see the histogram of the in-situ open ocean salinities collected by Argo floats in Fig. 2 (a) and Dinnat et al. [19] for the processing of the

histogram data). Since the old measurements [12] had only one salinity value (35 psu) in this range, new batches of seawater samples were purchased from Ocean Scientific International Limited (OSIL). This special order included 34 and 36 psu seawater samples to improve the density of measurements near 35 psu. The measurement points are indicated in Fig. 2 (a) with red and blue arrows representing the coverage of original and new data. In addition, seawater samples at 10 and 20 psu were purchased for measurements of regions having fresher seawater, for instance, coastal areas and large river mouths.

The new measurements of 10, 20 and 34 psu were made for the temperature ranging from 0°C to 30° C and the measurements of 36 psu were made for temperatures ranging from 10°C to 30° C. These experiments were conducted using an upgraded system [20]. New thermistors were purchased that had an accuracy of 0.01°C from -5°C to 35°C. The old network analyzer was replaced by a newer model, Keysight model E5072A, with better frequency stability that reduced the standard deviations of new measurement data. Some of the old measurement points were repeated with the new system and the differences were small. At each salinity and temperature, the averaged result was obtained from at least three different measurements. The averaged results for the new measurements were tabulated in Appendix A, Table A.1. The data for each individual measurement are documented at NASA URL (under construction, will be accomplished during reviewing).

The new datasets also include low temperature measurements for the study of cold oceans, where the sensitivity of the measured brightness temperature to salinity is weakest [21]. Such sensitivity drops from 0.5 K/psu to 0.3 K/psu, when SST decreases from 15°C to 5°C [22]. Since the brightness temperature is a function of the dielectric constant of seawater, a small change in the dielectric constant of seawater will cause a relatively large difference in retrieved salinity at low temperature. Therefore, it is important to have an accurate dielectric model for low temperature. Fig. 2 (b) shows the number of in-situ data collected by Argo below 5°C. It is seen that most of the cold oceans have salinity ranging from 32 to 35 psu with a peak at around 34 psu. Since the freezing point of seawater ranges from -1.5° to -2° C depending on the salinity of seawater, the low temperature measurements were made at -1.5, -1, 2 and 3°C for seawater with salinities of 30, 34 and 35 psu. The main purpose of making dielectric measurements of 30 psu at low temperatures is to provide a reference for the future study of ocean with melted ice, which usually has lower salinity. These low temperature measurement data are tabulated in Appendix A, Table A.2.

Besides seawater, the dielectric measurements were also made for distilled water at 1.4134 GHz from 0°C to 35°C in a 5°C interval. Similar to the seawater measurements, the distilled water was pushed through a capillary tube by nitrogen during the measurements. The freezing point of distilled water, therefore, is below 0ºC due the capillary freezing point depression [23]. The purpose of measuring the distilled

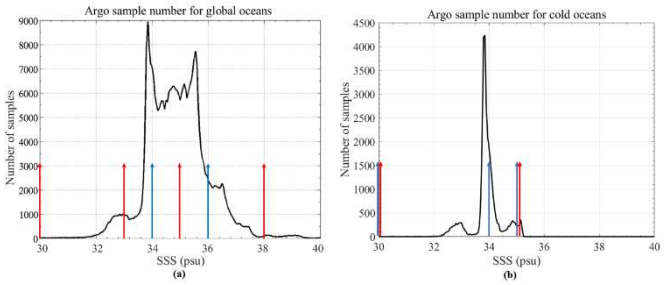

Fig. 2 Histogram of the salinity sample number from Argo in-situ data over the global ocean: (a) The number of occurrences of SSS for all temperatures in the global oceans; (b) The number of occurrences of SSS for oceans at low temperature (below 5° C) only. For both plots, the red arrows represent the salinity at which the original data points were acquired for the GW2017 model. The blue arrows represent the new data points added for the model presented in this paper.

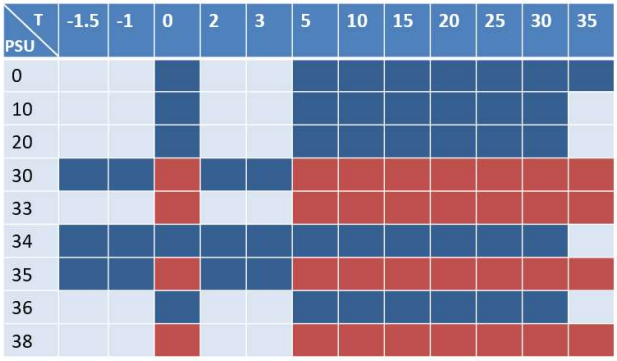

Fig. 3 Summary of measurement data points (blue blocks: new measurements made through 2018-2020; red blocks: original measurements made before 2017 [12])

water dielectric constant is to develop a Debye model for distilled water. The Debye model for seawater must then approach the distilled water model as salinity tends to zero. The distilled water dielectric constant data are tabulated in Appendix A, Table A.3.

The measurement data are summarized in Fig. 3, where the blue blocks represent the measurement made after year 2018 and the red blocks represent the original measurement data documented in [12].

III. Development of the Model Function using Debye Form plus a Conductivity Term

This section introduces the development of the seawater dielectric model function based on all the data tabulated in Appendix A together with the original data documented in [12]. The Debye model of seawater will be developed based on the Debye model of distilled water. The goal is to develop a physical-based model which fits closely to the lab measurement data at L-band.

A. Development of the Debye model function of distilled water

The Debye model of distilled water can be written as:

$$\varepsilon_{dw}(T) = \varepsilon_{\infty} + \frac{\varepsilon_{s-dw}(T) - \varepsilon_{\infty}}{1 + j\omega\tau(T)} \tag{1}$$

where $\varepsilon_{\infty} = 4.9$ is the dielectric constant of distilled water at infinite frequency [14]; $\omega = 2\pi f_0$, here, $f_0 = 1.4134$ GHz ; $\varepsilon_{s-dw}(T)$ is the static dielectric constant and $\tau(T)$ is the

relaxation time, both expressions are a function of temperature, T. Hereinafter, T is evaluated based on the unit of degree Celsius (°C).

It is seen from (1) that only two unknown parameters, $\varepsilon_{s-dw}(T)$ and $\tau(T)$, need to be evaluated from the dielectric constant measurement data for distilled water tabulated in Table A.3. Here, both ε_{s-dw} and τ are real parameters. If ε_{dw} is expressed as $\varepsilon_{dw} = \varepsilon'_{dw} - j\varepsilon''_{dw}$, (1) can be written as:

$$\varepsilon'_{dw}(T) = \varepsilon_\infty + \frac{\varepsilon_{s-dw}(T) - \varepsilon_\infty}{1+[\omega\tau(T)]^2} \quad \varepsilon''_{dw}(T) = \frac{\omega\tau(T)[\varepsilon_{s-dw}(T) - \varepsilon_\infty]}{1+[\omega\tau(T)]^2}, \tag{2a-b}$$

where $\varepsilon'_{dw}(T)$ and $\varepsilon''_{dw}(T)$ are the real and imaginary parts of the dielectric constant of distilled water at temperature T.

Using eqs. (2a-b), ε_{s-dw} can be eliminated yielding the following equation for the relaxation time in terms of the measured data:

$$\tau(T_j) = \frac{\varepsilon''_{dw}(T_j)}{\omega\left[\varepsilon'_{dw}(T_j) - \varepsilon_\infty\right]}, \tag{3}$$

where the temperature T has been evaluated at the measurement points T_j.

Therefore, the values of τ at T_j can be computed by using (3). A Least-squared method (LSM) has been used to fit the values of $\tau(T_j)$ to a third-order polynomial as a function of temperature T based on the methodology and criteria of data fitting given in Appendix B. The expression obtained for $\tau(T)$ is:

$$\tau(T) = 1.75030\text{E-}11 - 6.12993\text{E-}13\cdot T + 1.24504\text{E-}14\cdot T^2 - 1.14927\text{E-}16\cdot T^3. \tag{4}$$

The fitted $\tau(T)$ is plotted in Fig. 4 (a) with the results computed from measurement data. In order to estimate the closeness of fit, root mean square error (RMSE) and mean absolute percentage error (MAPE) between the modelled results and data are computed. The value of RMSE provides a measure of the difference between the data and model, whereas the value of MAPE estimates the relative deviation between the data and model, which is more conclusive for small parameters, e.g. relaxation time. The formulas for RMSE and MAPE are given in Appendix B. For the relaxation time, the RMSE is found to be 7.18E-14 and the MAPE is found to be 0.53%.

With a known relaxation time, the expression for the static dielectric constant $\varepsilon_{s-dw}(T)$ can be found by fitting a polynomial to the measured $\varepsilon_{s-dw}(T_j)$, which can be obtained from the measured ε'_{dw} at temperature T_j based on (2a).

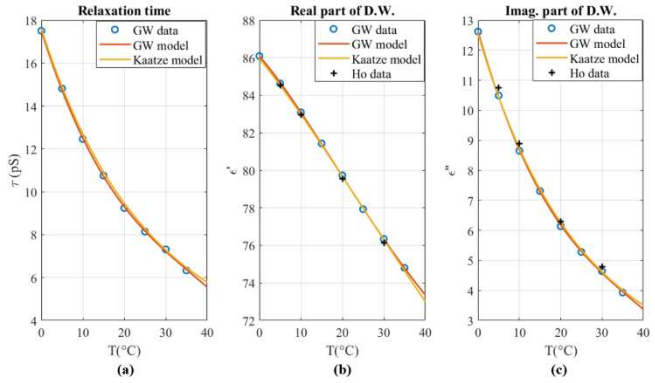

Fig. 4 Data fitting for distilled water dielectric constant: (a) relaxation time; (b) real part; (c) imaginary part. GW model – distilled water model given in this paper; Kaatze – the model given in [24]; Ho data – the data given in [8]

Following the criteria given in Appendix B, a third-order polynomial is chosen to represent the static dielectric constant ε_{s-dw} as a function of T. The constant term in the expression is determined directly from the distilled water measurement result $\varepsilon'_{dw}(T=0)$ in order to reduce the number of coefficients in data fitting. The other terms in the polynomial are determined by the least square fit to the measured $\varepsilon_{s-dw}(T_j)$. Finally, the expression for $\varepsilon_{s-dw}(T)$ is given as:

$$\varepsilon_{s-dw}(T) = 8.80516\text{E+}01 - 4.01796\text{E-}01\cdot T - 5.10271\text{E-}05\cdot T^2 + 2.55892\text{E-}05\cdot T^3 \tag{5}$$

The modeling results of the real and imaginary parts of distilled water are obtained using (4) for $\tau(T)$ and (5) for $\varepsilon_{s-dw}(T)$. The fitted results are plotted with the measurement results in Fig. 4 (b) and (c) for the real and imaginary parts, respectively. The RMSEs between the fitted and the measured results are 4.30E-2 and 4.61E-2 and the MAPEs are 0.03% and 0.52% for the real and imaginary parts of the permittivity of distilled water, respectively. It has been found that the condition numbers for the inversion of both $\tau(T)$ and $\varepsilon_{s-dw}(T)$ are not large, which implies that the results are not sensitive to noise in the measurement data.

The measured distilled water results are compared with the Kaatze model [24] and the measured data from Ho et al. [8], which are made at 1.43 GHz using a reflection type cavity. Compared with the Kaatze model, the only noticeable difference for τ and the permittivity of distilled water occurs at T = 40°C. Compared with Ho et al.'s data, the real parts are in good agreement while the imaginary part has a 0.1-0.2 difference. This deviation may be due to the difference in measurement frequency, the difference in distilled water samples and the differences in measurement techniques.

B. Development of the Debye model function of seawater

Based on the physical property of seawater reported in [25], the relaxation time of distilled water is not much affected by the addition of salt. This assumption means that the expression of $\tau(T)$ can also be employed in the seawater dielectric model.

Therefore, the Debye model for the seawater dielectric constant can be expressed by:

$$\varepsilon_{sw}(S,T) = \varepsilon_{\infty} + \frac{\varepsilon_{s-dw}(T)R_{sw-dw}(S,T) - \varepsilon_{\infty}}{1 + j\omega\tau(T)} - \frac{j\sigma(S,T)}{\omega\varepsilon_0}, \quad (6)$$

where S is the salinity of seawater in psu; ε_0 is the dielectric constant of free space; $\varepsilon_{s-dw}(T)$ and $\tau(T)$ are the static dielectric constant and relaxation time of distilled water respectively, as given in (4) and (5); $R_{sw-dw}(S,T)$ is an additional factor in the static dielectric constant of seawater due to the presence of ions; $\sigma(S,T)$ is the conductivity of seawater. Here it is assumed that $R_{sw-dw}(S,T)$ and $\sigma(S,T)$ are real functions.

To validate the assumption that the relaxation time, τ, can be expressed simply as a function of T, the percentage difference between $\tau(T)$ in GW distilled water model and $\tau(S,T)$ in KS model is plotted in Fig. 5 for T ranging from 0º C to 35º C and S (for KS model) ranging from 0 to 30 psu. It is seen that the variation of S does not have a significant effect on τ. The τ value of GW model is very close to KS model regardless of the value of salinity. The biggest deviation in τ, which is about 2% between GW model and KS model, occurs at T = 0ºC and S = 30 psu. Note that the accuracy of the Debye model of seawater at 1.4134 GHz will not be affected by the assumption that the relaxation time is independent of S. This is because the other two parameters, $R_{sw-dw}(S,T)$ and $\sigma(S,T)$, will be determined by fitting to the seawater dielectric data made at 1.4134 GHz. Any errors in $\tau(T)$ will be compensated by $R_{sw-dw}(S,T)$ and $\sigma(S,T)$ at 1.4134 GHz through the data fitting procedure.

In (6), $R_{sw-dw}(S,T)$ can be written as [25],

$$R_{sw-dw}(S,T) = 1 - S \cdot \alpha(S,T) \quad (7)$$

where α is a polynomial in S and T. It is seen from (7) that the expression for $R_{sw-dw}(S,T)$ assures that the real part of the seawater dielectric constant converges to the real part of distilled water dielectric constant when $S = 0$.

The values of $R_{sw-dw}(S,T)$ at the measurement point (S_i,T_j) can be obtained from the real part of (6) and (2a), which is given:

$$R_{sw-dw}(S_i,T_j) = \frac{\left[\varepsilon'_{sw}(S_i,T_j) - \varepsilon_{\infty}\right]\left[1 + \omega^2\tau^2(T_j)\right] + \varepsilon_{\infty}}{\varepsilon_{s-dw}(T_j)} \quad (8)$$

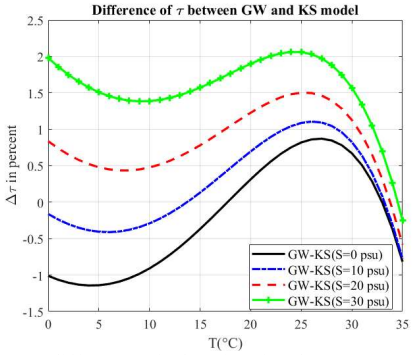

Fig. 5 Percentage difference of relaxation time between GW and KS model

where $\tau(T_j)$ and $\varepsilon_{s-dw}(T_j)$ can be computed from (4) and (5), respectively; $\varepsilon'_{sw}(S_i,T_j)$ is the real part of the measured seawater dielectric constant at salinity S_i and temperature T_j. These measurement results are given in [12], and here in Table A.1 and Table A.2 for additional salinity S_i and temperature T_j.

To determine the expression for $R_{sw-dw}(S,T)$, the right-hand-side of (8) is computed based on the measurement data and plotted in Fig. 6 (a) and (b) as a function of T and S, respectively. It is seen that the temperature dependence in $R_{sw-dw}(S,T)$ is approximately linear while the salinity dependence in $R_{sw-dw}(S,T)$ is slightly curved. Therefore, the initial guesses for the highest orders of T and S are 1 and 2, respectively. In addition, Fig. 6 (b) shows that the dispersion between different temperatures increases as salinity becomes higher. This means there is at least one term that contains the product of salinity and temperature, ST, in the expression of $R_{sw-dw}(S,T)$. Finally, the highest order of S was found to be 3 and the highest order of T was found to be 1 to provide a good representation for $R_{sw-dw}(S,T)$ based on the criteria given in Appendix B. The expression of $R_{sw-dw}(S,T)$ is given as:

$$R_{sw-dw}(S,T) = 1 - S \cdot (3.97185\text{E-}03 - 2.49205\text{E-}05 \cdot T - 4.27558\text{E-}05 \cdot S + 3.92825\text{E-}07 \cdot ST + 4.15350\text{E-}07 \cdot S^2). \quad (9)$$

The modeled results are plotted in Fig. 6 (c) and (d), which show that R_{sw-dw} is approximately linear in salinity and temperature. There is good agreement between the modeled $R_{sw-dw}(S,T)$ and the measured data. It is seen that the noise due to uncertainties in the measurements, e.g. the salinity dependence for seawater having 34 - 38 psu salinities, is smoothed by the model.

Based on the expression of the imaginary part of dielectric constant given in (6), the conductivity term $\sigma(S,T)$ at the measurement point (S_i,T_j) can be computed by:

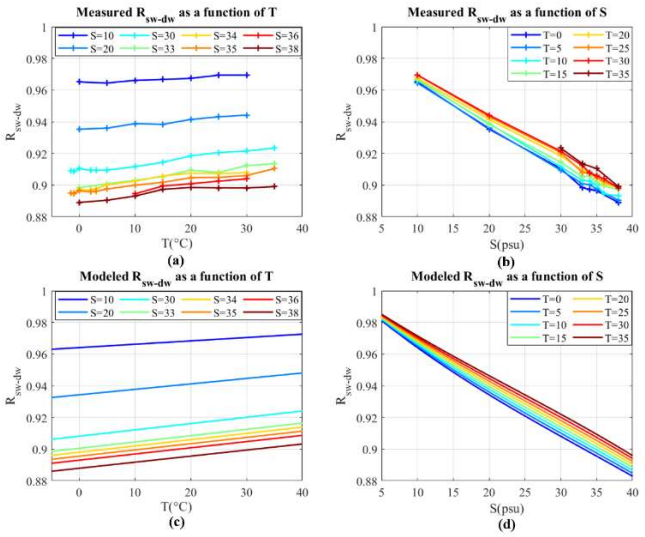

Fig. 6 Data fitting for $R_{sw-dw}(S,T)$. (a) measured $R_{sw-dw}(S,T)$ as a function of T; (b) measured $R_{sw-dw}(S,T)$ as a function of S; (c) modeled $R_{sw-dw}(S,T)$ as a function of T; (d) modeled $R_{sw-dw}(S,T)$ as a function of S.

$$\sigma(S_i,T_j)=\omega\varepsilon_0\varepsilon''_{sw}(S_i,T_j)-\frac{\omega^2\varepsilon_0\tau(T_j)\cdot[\varepsilon_{s-dw}(T_i)R_{sw-dw}(S_i,T_j)-\varepsilon_\infty]}{1+\omega^2\tau^2(T_j)}, \quad (10)$$

where $\varepsilon''_{sw}(S_i,T_j)$ is the imaginary part of the measurement data at salinity S_i and temperature T_j; $\tau(T_j)$, $\varepsilon_{s-dw}(T_j)$ and $R_{sw-dw}(S_i,T_j)$ can be computed from (4), (5) and (9), respectively. The measured results of $\sigma(S_i,T_j)$ are plotted in Fig. 7 (a) and (b) as a function of T and S, respectively.

Note that $\sigma(S,T)$ needs to be nulled at S = 0 since the conductivity of distilled water is close to 0. Therefore, $\sigma(S,T)$ can be expressed as: $\sigma(S,T)=S\cdot\beta(S,T)$ where the expression for $\beta(S,T)$ can be determined by fitting a polynomial to the measurement results. It can be seen from Fig. 7 (a) and (b) that the conductivity term $\sigma(S,T)$ has a slightly nonlinear dependence on salinity and temperature. Since the terms containing T in the expression of $\sigma(S,T)$ are nulled at T = 0°C, the measurement data at 0°C are used to determine the coefficients of the terms that only contain salinity. A third-order fit was found to be a good representation for $\sigma(S,0)$ based on the criteria given in Appendix B; the expression for σ is:

$$\sigma(S,0)=\ 9.50470\text{E-}02\cdot S-4.30858\text{E-}04\cdot S^2+2.16182\text{E-}06\cdot S^3. \quad (11)$$

Although the expression for $\sigma(S,0)$ has been determined, the choice of the highest order of T in the expression is not clear. In order to further determine the expression for $\sigma(S,T)$, the ratio of $\sigma(S,T)$ to $\sigma(S,0)$, which is denoted as $R_\sigma(S,T)$, has been computed for all measurement temperatures that are greater than 0°C.

Based on the measurement data, the results of $R_\sigma(S,T)$ are plotted in Fig. 7 (c) and (d) as a function of temperature and salinity, respectively. As expected, Fig. 7 (c) shows that $R_\sigma(S,T)$ has a nonlinear dependence on T. This dependence can be expressed by a polynomial of T in the expression of $R_\sigma(S,T)$. In Fig. 7 (c) , the curves of $R_\sigma(S,T)$ have a good convergence for 30-38 psu seawater while the slope of $R_\sigma(S,T)$ is slightly different for seawater having salinities of 10 and 20 psu. This difference is also shown in Fig. 7 (d). If all the lines in Fig. 7(d) were perfectly flat, $R_\sigma(S,T)$ would only be a function of T, independent of S. This assumption, however, is not the case in Fig. 7 (d) since the lines for $T >$ 0°C has a small negative slope for $S <$ 30 psu. This indicates that there should be at least one small correction term, which contains salinity S, in the expression of $R_\sigma(S,T)$.

With the definition of $R_\sigma(S,T)$, the expression of $\sigma(S,T)$ can be written as:

$$\sigma(S,T)=\sigma(S,0)\cdot R_\sigma(S,T)=\sigma(S,0)\cdot\left[1+T\cdot\Gamma(S,T)\right] \quad (12)$$

where $R_\sigma(S,T)$ is expressed as $1+T\cdot\Gamma(S,T)$ to assure that $\sigma(S,T)$ converges to the expression of $\sigma(S,0)$ when T = 0°C. Based on the previous discussion, $\Gamma(S,T)$ contains a polynomial of T plus correction terms for salinity dependence slope shown in Fig. 7 (d). A second-order polynomial of T and S has been found to be a good representation for $\Gamma(S,T)$. Finally, $R_\sigma(S,T)$ can be expressed as:

$$R_\sigma(S,T)=1+T\cdot(\ 3.76017\text{E-}02+6.32830\text{E-}05\cdot T+4.83420\text{E-}07\cdot T^2-3.97484\text{E-}04\cdot S+6.26522\text{E-}06\cdot S^2). \quad (13)$$

Eqs. (11), (12) and (13) together provide the expression of $\sigma(S,T)$. The modeled results are plotted in Fig. 8. Good agreement can be observed between the model and the measured data. The modeling of $\sigma(S,T)$ also corrects some noise of data due to measurement uncertainties, e.g. conductivity of seawater at 20 psu salinity and 15° C.

As given by eqs. (1) – (13), the GW Debye model, which will be referred to as the GW2020 model, has been developed. The RMSEs between the measurement data and GW2020 model are 0.11 and 0.31 and the MAPEs are 0.12% and 0.39%, respectively. The main reason for the larger RMSE in the imaginary part is that the dynamic range of ε'' is about 3 times larger than the dynamic range of ε' for the studied temperature and salinity region (see the data in Appendix A). The RMSEs obtained for the previous GW2017 model is 0.09 for the real part and 0.17 for the imaginary part. Although GW2020 model has slightly larger RMSEs than GW2017 model, its behavior is more stable as shown in the rest of the paper. A summary of the expressions of parameters in the GW2020 model function is given in Appendix C.

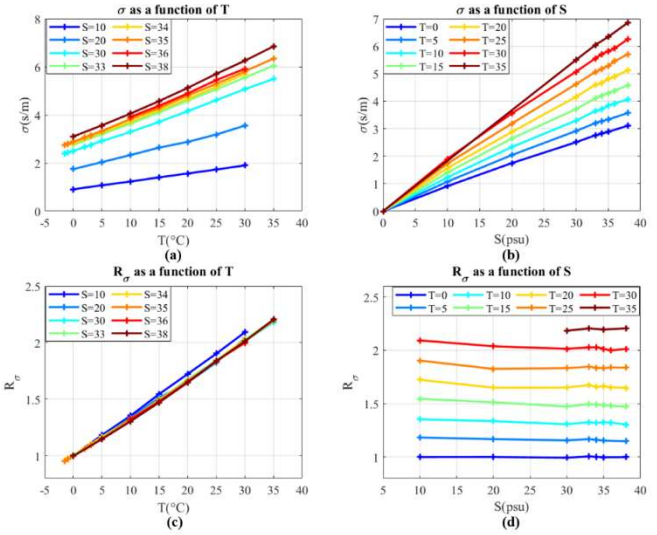

Fig. 7 Measured results. (a) and (b): $\sigma(S,T)$ as a function of T and S, respectively; (c) and (d): $R_\sigma(S,T)$ as a function of T and S, respectively

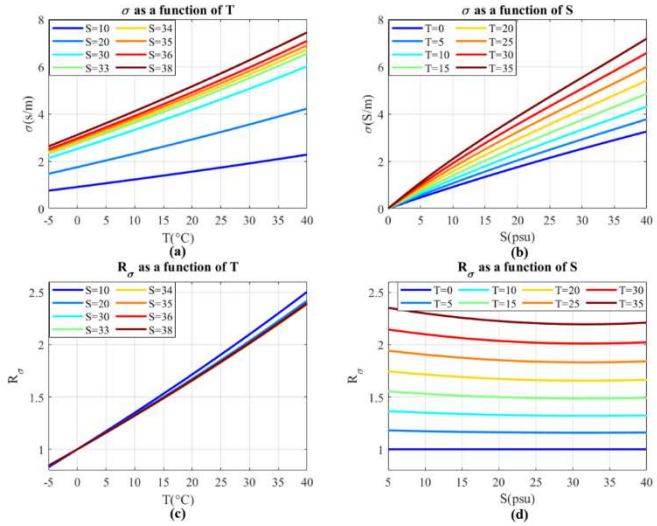

Fig. 8 Modeled results. (a) and (b): $\sigma(S,T)$ as a function of T and S, respectively; (c) and (d): $R_\sigma(S,T)$ as a function of T and S, respectively.

Compared with the GW2017 model, the GW2020 model prevents the overfitting problems by the following methodologies:

1. It uses a more complete dataset, which provides more data to reduce the condition number in the inversion, as well as, improve the accuracy of the model function.
2. A physical-based Debye structure is used to reduce the number of coefficients determined by one data fitting procedure. The expressions of the relaxation time τ and the static dielectric constant, $\varepsilon_{s-dw}(T)$ are determined first for the distilled water. These parameters were then employed in the Debye model of seawater. The expressions of other parameters in the seawater Debye form, i.e. static dielectric constant and conductivity term, are determined by a careful analysis of the plots of measurement results. The number of coefficients, again, is strictly constrained in the data fitting procedure to avoid overfitting issue.

C. Model Comparisons

This section shows comparisons between the KS, the MW and the GW2020 model functions. Considering that at L-band the conductivity is the dominant part of the imaginary part of dielectric constant, the first comparison is made for the conductivity terms, σ, among three models. Since the SSS of Open Ocean can vary from 30 to 38 psu, the comparison is made for the same salinity range. The KS model and the MW model used the conductivity model developed by Stogryn et al. at different periods (KS model used [13], MW used [6]). These conductivity models are developed based on actual conductivity measurements, which generally have different mechanism and setup from the dielectric measurements. The difference in σ between the GW2020, the KS and the MW models are plotted in Fig. 9.

It is seen from the figure that the difference between the GW2020 model and the other two models is approximately within 0.04 over the temperature ranging from -2 to 37 degree. In general, the GW2020 predicts slightly lower σ. The similarity between two figures is no surprise since both the KS and the MW models used Stogryn's results.

The difference between the real and imaginary parts of three model functions are plotted in Fig. 10 as a function of temperature for different salinities. It is seen that both the real and imaginary parts of the GW2020 model have a good convergence between salinities when compared with the other two models. The GW2020 model predicts higher ε' at low temperature and lower ε' at high temperature when compared with the KS model while it predicts higher ε' as temperature goes higher when compared with the MW model. For the imaginary part, the GW2020 model generally has higher value at low temperature and lower value at high temperature when compared with the other two model functions.

To investigate the combined effect of real and imaginary parts of the dielectric constant model in salinity retrieval, the brightness temperatures in v-pol for a flat surface are obtained by:

$$T_{bv}(\varepsilon(S,T),T) = (1-\left|\Gamma_v(\varepsilon(S,T))\right|^2)T \tag{14}$$

where $\varepsilon(S,T)$ represents the dielectric constant model function used in the algorithm; $\Gamma_v(\varepsilon(S,T))$ is the v-pol Fresnel reflection coefficient that can be expressed by:

$$\Gamma_v(\varepsilon(S,T)) = \frac{\varepsilon(S,T)\cos\theta - \sqrt{\varepsilon(S,T)-\sin^2\theta}}{\varepsilon(S,T)\cos\theta + \sqrt{\varepsilon(S,T)-\sin^2\theta}}. \tag{15}$$

Here, $\theta = 40°$ is the incident angle chosen to be representative of the antenna on satellites (e.g. this is the angle for the sensor on SMAP mission and the Aquarius middle beam radiometer). Note that the value of θ has a very small effect on the difference of brightness temperature between model functions. The differences in T_b between the GW2020 and KS, MW model functions are shown in Fig. 11 (a) and (b), while the differences in T_b between the GW2017 and the other two model functions are given in Fig. 11 (c) and (d).

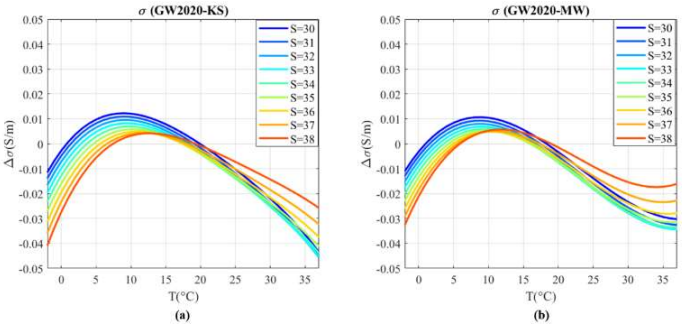

Fig. 9 Comparison of the conductivity term between different model functions. (a) Difference between GW2020 and KS models; (b) Difference between GW2020 and MW models

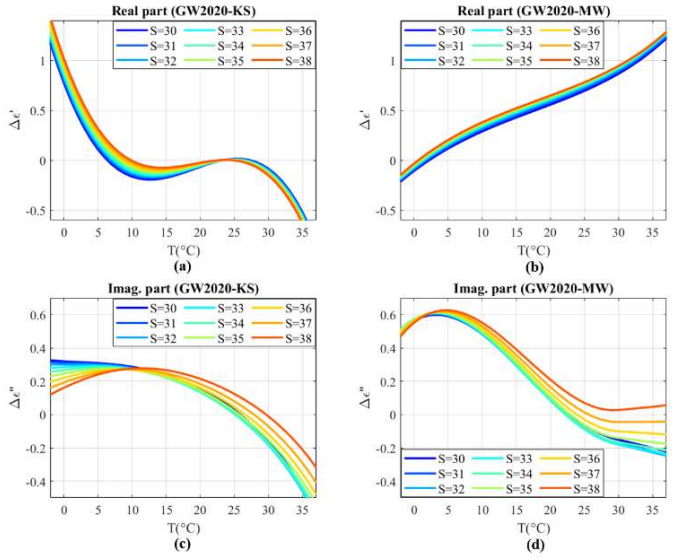

Fig. 10 Comparison of the complex dielectric constants between different model functions. (a) and (c): difference between the real and imaginary part of GW2020 and KS; (b) and (d): difference between the real and imaginary part of GW2020 and MW.

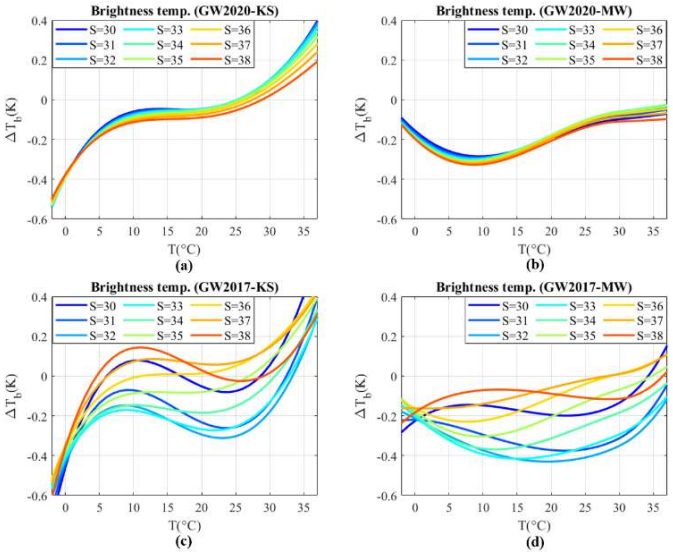

Fig. 11 Comparison of flat surface T_b (V-pol, EIA = 40°) between different model functions. (a) and (b) comparison between GW2020 and KS, MW models; (c) and (d) comparison between GW2017 and KS, MW models.

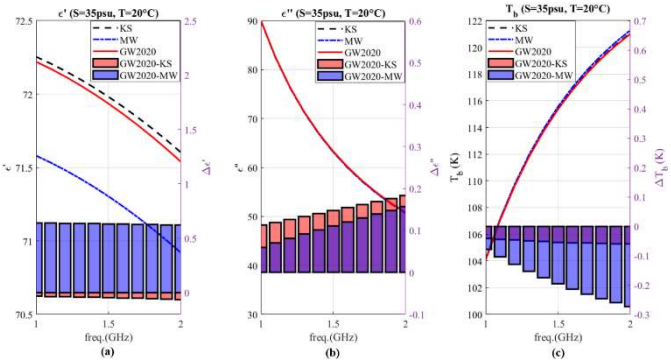

Fig. 12 Comparison of the dielectric constant models as a function of frequency, where the y-axis on the right represents the scale of the difference. Note that the purple bars representing the overlapped area for the red bars (GW2020-KS) and blue bars (GW2020-MW). (a). ε' for seawater having 35 psu salinity at 20° C, (b) ε'' for seawater having 35 psu salinity at 20° C, (c) T_b for seawater having 35 psu salinity at 20° C.

It is seen from Fig. 11 (a) and (b) that the difference in T_b between the GW2020 and the other two models is very consistent between salinities. The dispersion between salinities for the GW2020 model is much smaller than it is for the GW2017 model function. The GW2020 model predicts lower T_b at low temperature and higher T_b at high temperature when compared with KS model function, whereas the GW2020 model estimates slightly lower T_b across the whole temperature range when compared with the MW model. In the salinity retrieval process, the absolute bias can usually be removed through calibration, which would simply shift the curves up and down. By removing 0.2 K absolute bias between the GW2020 model and the MW model, the difference between these two models is generally within ±0.1 K for most of the temperature points. Note that 0.1 K is the radiometric accuracy that is required for salinity retrievals.

The comparison has also been made between the three models as a function of frequency. The results are plotted in Fig. 12 for seawater with a salinity of 35 psu at 20° C. In the figure, the curves represent the values (left y-axis) and the bars represent the differences (right y-axis). It is seen that although the GW2020 model function has been developed based on the measurements made at a single frequency (1.4134 GHz), the differences between the GW2020 and the other two models are very small and consistent from 1 to 2 GHz. Note that the three lines are overlapped in Fig. 12 (b); this indicates that the imaginary parts of the three model functions are in good agreement.

IV. Application of GW2020 Model Function on Salinity Retrieval

This section introduces the effect of using different model functions on the retrieval of salinity. In this section, SST (for Sea Surface Temperature) and SSS (for Sea Surface Salinity) are used in places of temperature T and salinity S, since this notation is commonly used in the literature for remote sensing of oceans. The retrieval process employs the entire Aquarius dataset from 2011 to 2015. The SSS retrieval uses Aquarius flat surface Brightness Temperature T_b, which is obtained

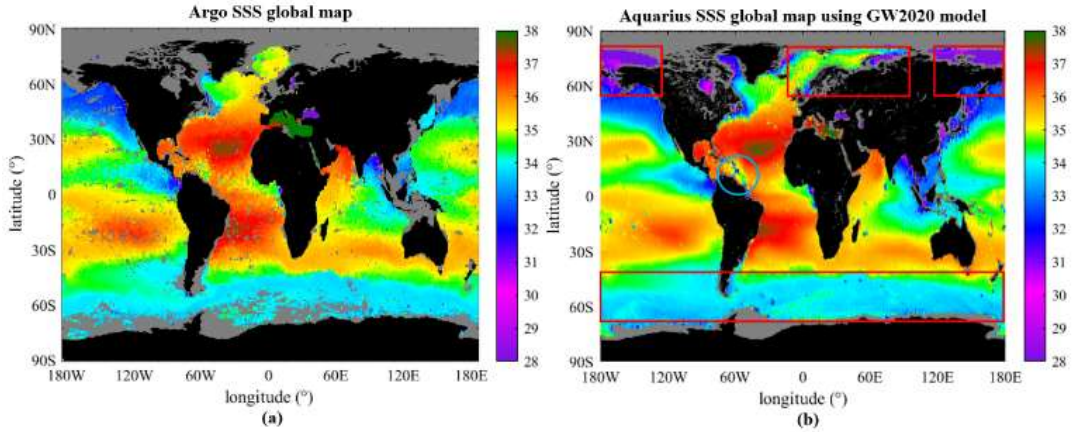

Fig. 13 SSS global map for (a) in-situ data collected by Argo floats and (b) retrieved SSS from Aquarius observation using GW2020 model function.

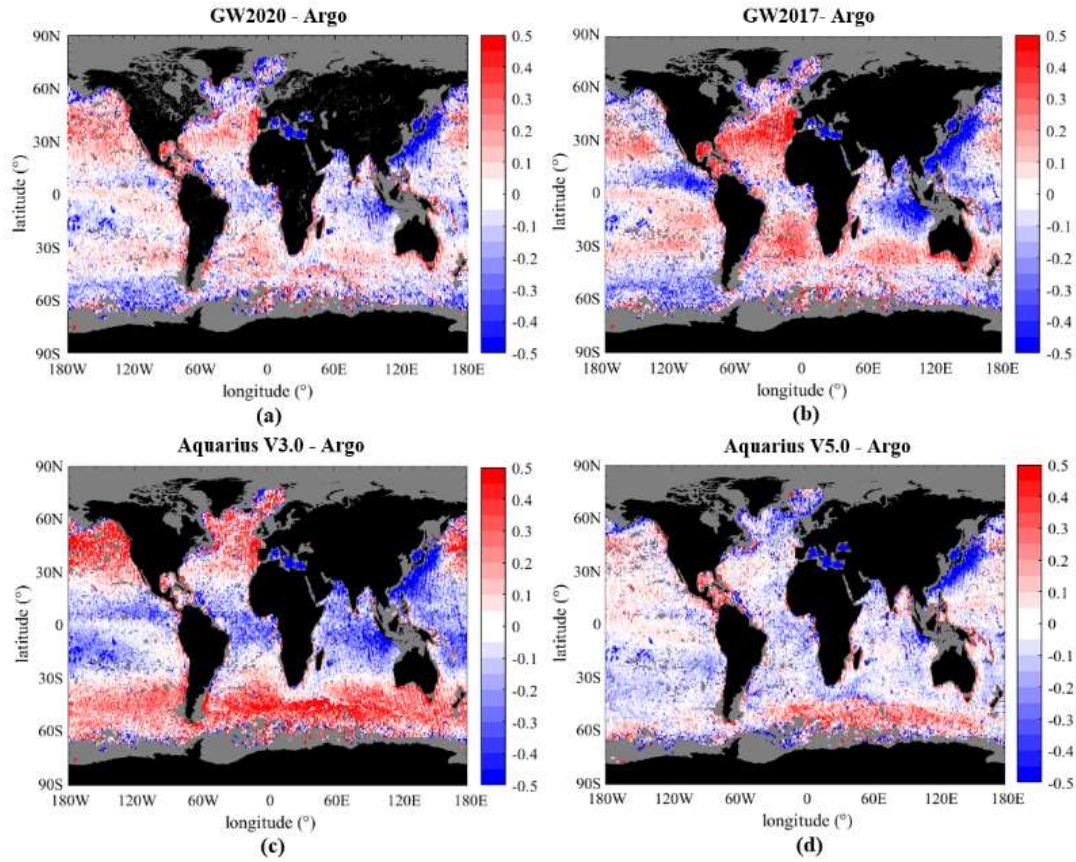

Fig. 14 ΔSSS global map for (a) Aquarius V5.0 – Argo; (b) GW2017 – Argo; (c) Aquarius V3.0 – Argo and (d) GW2020 – Argo

from a large number of transformations from the original sensor measurements. Spurious radiation sources are removed (e.g. wind, atmosphere, ionosphere, galaxy) or corrected for (e.g. Faraday rotation) through the transformation process. The effects of the antenna patterns (polarization mixing, convolution of the scene [26]) are also considered in the transformation. More details on this processing can be found in [27]. The Aquarius retrieval algorithm V3.0 (doi: 10.5067/AQUAR-2S1PS) is processed using the three different model functions (KS, MW and GW2020) with other parameters remaining the same, e.g. surface roughness correction and atmospheric attenuation. The V3.0 algorithm is chosen because it does not contain the empirical SST-dependent correction based on the MW model function; this correction has been included in the later versions of the retrieval algorithm [27][28]. Note that the retrieval algorithm also includes a global bias adjustment which is affected by the choice of model function and is recalibrated for each model function. The retrieval algorithm has been run for the entire Aquarius dataset to produce almost 4 years of SSS retrievals along the satellite beam tracks at a time resolution of 1.44

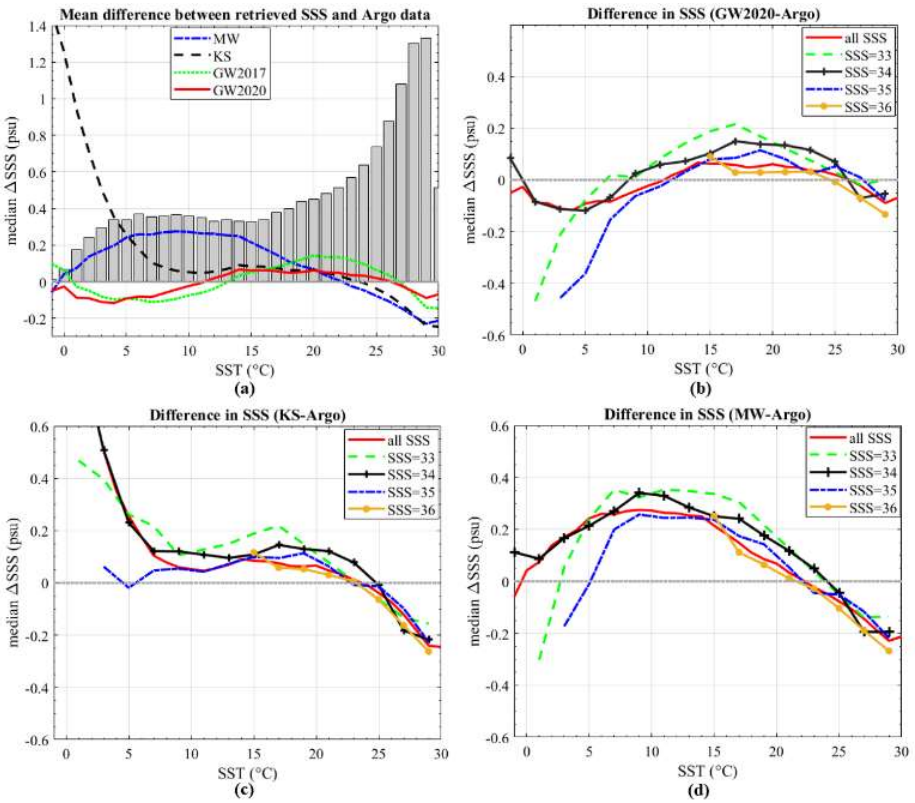

Fig. 15 ΔSSS as a function of SST. (a): Average ΔSSS of all different SSS; (b): ΔSSS between MW and Argo; (c): ΔSSS between KS and Argo; (d): ΔSSS between GW2020 and Argo

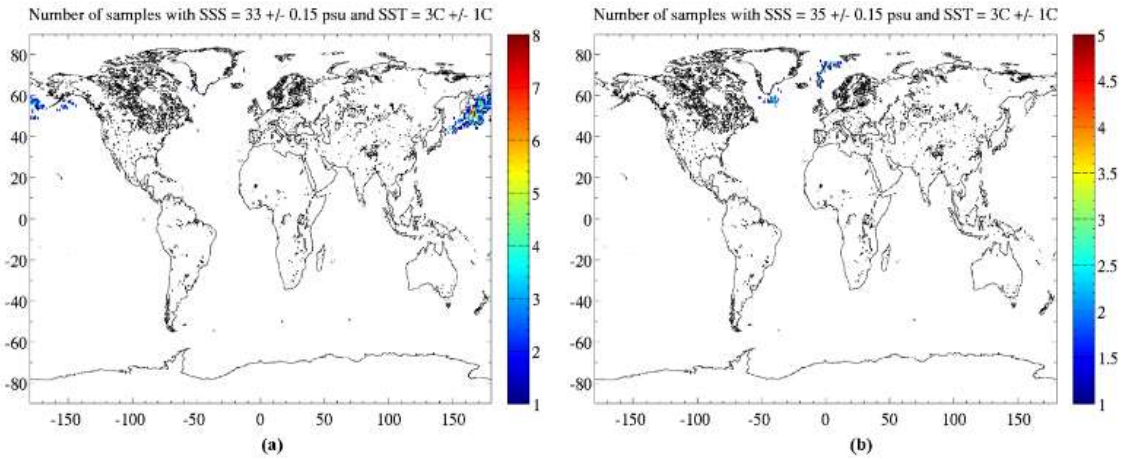

Fig. 16 Locations of in-situ samples at low temperature for: (a) 33 psu (b) 35 psu

second (about every 10 km along track). The retrieved SSS is then gridded into global monthly maps at 1° × 1° resolution in latitude × longitude using drop-in-a-bucket averaging. The retrieved SSS are compared to in-situ SSS observation from the Argo network of free-drifting profiling floats [29]. There are about 4000 Argo floats that surface every 10 days from 2000 m deep and provide quasi-global coverage of the ocean surface. We use only observations from 10 m deep or less to compare to the satellite SSS. The Argo samples are also re-gridded monthly at 1° resolution, similar to the resolution of satellite SSS. More details can be found in [19].

The retrieved SSS global map using GW2020 model is shown in Fig.13 along with the Argo SSS global map. The color bar shows the SSS in psu. All the maps reported in this paper are the average of all the monthly maps during the Aquarius V3.0 availability (September 2011 – May 2015). It is seen from Fig.13 that the retrieved SSS map has a finer resolution than the Argo SSS map. Compared with Argo data, the retrieved SSS contains some additional information, e.g. the Amazon River runoff (blue circle in Fig.13 (b)), the SSS for Cold Oceans (red squares in Fig.13 (b)). This additional information is very valuable for the study of climate change and global water cycle.

The difference between the retrieved SSS and the in-situ SSS collected by the Argo floats (referred to as ΔSSS in this paper) has also been evaluated and plotted as a global map in Fig. 14. In this figure, the ΔSSS is obtained by using GW2017, GW2020 and MW model functions based on Aquarius V3.0 retrieval algorithm. The global ΔSSS is also retrieved using MW model function based on Aquarius V5.0 algorithm (doi: 10.5067/AQR50-2SOCS). As aforementioned, the Aquarius V3.0 product uses the MW model function with almost no other adjustment, so it is a good reference to evaluate this dielectric constant model. In contrast, the Aquarius V5.0 products have significant empirical adjustments to the retrieval aimed at mitigating an SST-dependent bias that was observed in Aquarius V3.0 using MW model function (see [19] for more details).

It is seen from Fig. 14 that the retrieved SSS using GW2020 model has the best agreement with in-situ data collected from Argo floats when compared with other products with no empirical adjustment. Compared with GW2017 and Aquarius V3.0 (i.e. MW model), the biases for the open oceans located from 50° N to 50° S latitude are significantly reduced by employing GW2020 model function. The retrieved SSS using GW2020 model function, however, slightly underestimates the SSS in the low Southern Oceans. This bias could be due to the high sensitivity of salinity to changes in the dielectric constant at low temperature. The Aquarius V5.0 product is slightly better than the retrieved SSS from GW2020 for the open oceans in Northern Hemisphere owing to its empirical adjustment that strongly mitigates the SST-dependent bias, and possibly an improved atmospheric correction model. For Southern Hemisphere, SSS retrieval using GW2020 model has advantages over Aquarius V5.0 products in certain regions.

The performance of different model functions is summarized in Fig. 15 by plotting the ΔSSS as a function of SST. Fig. 15 (a) gives a comparison of the averaged ΔSSS between different model functions. It shows that the GW2020 model generally has the best agreement with in-situ data from 5° to 30° C compared with other model functions. At low temperatures, GW2020 model slightly underestimates the salinities compared with in-situ data. This bias could be due to the high sensitivity of salinity to changes in the dielectric constant at low temperature. In addition, Fig. 15 (a) also shows a histogram of the number of samples collected by Argo floats at different SST (see the grey bars appearing behind the curves). It is seen that the number of in-situ samples at low temperatures is much lower than the samples at other temperatures, in particular, for 0°C and lower.

Fig. 15 (b), (c) and (d) show the dispersions in ΔSSS between salinities as a function of SST. It is seen that the KS, the MW and the GW2020 model functions have similar dispersions in ΔSSS. This similarity is simply a consequence of the dispersion plots shown in Fig. 11 (a) and (b). If we compare Fig. 15 (d) with Fig. 1 (b), we can observe that the GW2020 model has a much lower dispersion in ΔSSS than the GW2017 model. The reduced dispersion is due to that the GW2020 model function is less sensitive to noise in the data. At low temperatures, most of the contributions to ΔSSS are from seawater in the Southern Oceans which generally has a salinity of around 34 psu (see Fig.13). Note that this fact agrees with the number of sample statistics for in-situ data shown in Fig. 2 (b). The ΔSSS for 33 psu and 35 psu seawater at low temperatures is also plotted although the number of samples for these two salinities is much lower than 34-psu seawater at low temperatures. Relatively large deviations are seen for 33-psu and 35-psu seawater from 0 to 7°C in all three model functions. Further investigation has been done to locate the spots where salinities of 33 psu and 35 psu seawater at 3°C are found on the global salinity map and the results are plotted in Fig. 16. Most of the points for 33 psu and 35 psu seawater at 3° C are located on northern coastal regions (possibly near sea ice) where the land and ice contamination can have strong effect on the salinity retrieval. In addition, the locations for 33 psu seawater are near the coasts of East Asia, where the effect of RFI is relatively large. RFI can strongly affect the remote sensing of the ocean which may cause a bias in the retrieved salinity [30].

V. Conclusions

This paper discusses the development of a seawater Debye model at L-band (GW2020 model) based on lab measurements of seawater and distilled water. New seawater measurements have been made to expand the coverage of dataset for salinity ranging from 10 to 38 psu and temperature ranging from -1.5°C to 35°C. The Debye model of seawater is developed based on the Debye model of distilled water; this process ensures that the dielectric constant of seawater converges to distilled water when S=0. The parameters in the Debye form are expressed by polynomials of S and T, which are carefully determined by fitting to the expanded dataset. The choice of the highest order of S and T is dependent on the plot of measured data, the closeness of fit and the stability of the inversion for the coefficients.

The GW2020 model is applied on the salinity retrieval algorithm to obtain sea surface salinity from Aquarius satellite's data. Compared with other existing model functions, the retrieved SSS (with no empirical correction) from GW2020 model has overall the best agreement with in-situ data collected from Argo floats. The improved stability reduces the SSS dependent error of the model function, which results in a better performance on estimating the global SSS. In the future, the model function and salinity retrieval at low temperatures will be investigated to resolve the biases of retrieved salinity in the cold oceans. The GW2020 model will be used to retrieve SSS using SMAP data and other L-band satellites observations to further evaluate its performance.

APPENDIX A
NEW MEASUREMENT DATA

This appendix summarizes the averaged data for the measurements made during year 2018-2019. The individual measurement results are documented in detail at NASA URL (under construction).

Table A.1 GWU Seawater Permittivity Data (2018-2019)

Temp. (°C) \ PSU	10	20	34	36
0	83.09(±0.04)-j23.71(±0.07)	80.53(±0.15)-j33.97(±0.10)	77.26(±0.08)-j47.17(±0.32)	-
5	81.67(±0.00)-j23.74(±0.12)	79.27(±0.06)-j35.67(±0.06)	76.25(±0.03)-j50.99(±0.20)	-
10	80.29(±0.05)-j24.02(±0.22)	78.01(±0.06)-j37.78(±0.08)	74.99(±0.20)-j55.05(±0.08)	74.33(±0.15)-j57.57(±0.09)
15	78.70(±0.08)-j24.90(±0.11)	76.40(±0.05)-j40.41(±0.15)	73.74(±0.07)-j60.03(±0.15)	73.23(±0.17)-j62.27(±0.43)
20	77.09(±0.08)-j25.90(±0.08)	75.02(±0.05)-j42.42(±0.17)	72.32(±0.20)-j64.91(±0.14)	71.80(±0.02)-j67.78(±0.01)
25	75.61(±0.16)-j27.12(±0.07)	73.55(±0.14)-j45.49(±0.32)	70.77(±0.29)-j70.59(±0.13)	70.38(±0.23)-j74.07(±0.28)
30	74.02(±0.15)-j28.62(±0.26)	72.08(±0.20)-j49.53(±0.09)	69.30(±0.12)-j76.81(±0.31)	69.02(±0.12)-j79.41(±0.25)

Table A.2 Additional Low Temperature Seawater Permittivity Data (2018-2019)

Temp. (°C) \ PSU	30	34	35
-1.5	78.62(±0.10)-j42.53(±0.09)	-	77.40(±0.05)-j46.92(±0.28)
-1	78.46(±0.07)-j42.82(±0.23)	77.28(±0.07)-j46.82(±0.07)	77.25(±0.12)-j47.38(±0.05)
2	77.80(±0.13)-j44.50(±0.16)	76.74(±0.14)-j48.72(±0.16)	76.65(±0.14)-j49.42 (±0.14)
3	77.55 (±0.12)-j45.26(±0.25)	76.56(±0.11)-j49.62(±0.06)	76.41(±0.13)-j50.23(±0.23)

Table A.3 GWU Distilled Water Permittivity Data (2018-2019)

Temp. (°C)	Permittivity
0	86.09(±0.04)-j12.62(±0.03)
5	84.63(±0.06)-j10.49(±0.14)
10	83.09(±0.01)-j8.65(±0.04)
15	81.43(±0.08)-j7.31(±0.07)
20	79.74(±0.04)-j6.14(±0.18)
25	77.93(±0.11)-j5.28(±0.09)
30	76.35(±0.13)-j4.64(±0.10)
35	74.81(±0.16)-j3.93(±0.05)

APPENDIX B
DATA FITTING TECHNIQUE AND CRITERIA

In this appendix, the data fitting procedure for the Debye form of seawater dielectric constant is introduced. The expressions for each of the individual parameters in the Debye form can be determined by fitting a polynomial function of salinity (S) and temperature (T) to the measurement data. The goal of the data fitting is to ensure the stability of model as well as the closeness of fit between the model and data.

The Least Squared Method (LSM) has been employed in the data fitting. The fitting algorithm is similar to that used in Appendix A of [Zhou et al., 2017] except that the fitting in this article is unweighted. It has been found that the weighted fitting is unnecessary when the number of unknown coefficients is much smaller than the number of data points. This will be the case for the data fitting procedures in this paper.

What follows is a description of how any one of the Debye coefficients are determined. These coefficients are in general a function of S and T. The number of unknown coefficients, which will be denoted by L, needs to be carefully determined. Define the M and N as the lowest orders of S and T in the expression and P and Q as the highest orders of S and T in the expression. The number of unknown coefficients L can be represented by $L = (P - M + 1) \times (Q - N + 1)$. The value of M and N can be determined from the physical meaning of parameters. For instance, M = 1 and N = 0, i.e. the lowest orders of S and T are 1 and 0, can be used for the expression of the conductivity term $\sigma(S,T)$ since the conductivity of distilled water is 0 ($\sigma(0,T) = 0$).

The highest orders, P and Q, in the expression are determined comprehensively by taking all the following aspects into account:

1. The plots of the measured parameter as a function of S and T. The values of P and Q need to be large enough to ensure the polynomial can represent the shape of plotted curves.
2. The Root Mean Squared Error (RMSE) of the corresponding expression between measurement results and fitted polynomial. It has the following formula:

$$RMSE = \sqrt{\frac{1}{\mu}\sum_{i=1}^{u}\sum_{j=1}^{v}\left(\Delta y_{i,j}\right)^2} \tag{B.1}$$

where $\Delta y_{i,j}$ is the difference between the measurement and fitted results at S_i and T_j; μ is number of degrees of freedom that can be written as $\mu = K - L$. Here, u and v are the numbers of salinities and temperatures used in the measurements, $K = u \times v$ is the total number of measurement points.

Note that by increasing the number P and Q, the values of $\Delta y_{i,j}$ usually decrease, which means the model fits data closer. The value of μ, however, is also decreased. Thus the RMSE is not necessary made smaller by increasing P and Q in the polynomial. Another concern of increasing P and Q is the matrix will be ill-conditioned when the P and Q are too large. The matrix is then close to singular and the accuracy of fitting is undermined. Therefore, P and Q in the expression need to be kept as small as possible with an acceptable RMSE.

To further demonstrate how close the model fits the data, the mean absolute percentage error (MAPE) between the data and fitting is also computed based on the formula:

$$MAPE = \frac{1}{K}\sum_{i=1}^{u}\sum_{j=1}^{v}\frac{\left|\Delta y_{i,j}\right|}{y_{i,j}} \times 100\% \tag{B.2}$$

where $y_{i,j}$ is the value of the parameter at S_i and T_j and other parameters are the same as defined in (B.1).

3. The extrapolation of the model. Generally, the higher the order of the polynomial, the higher the possibility it will perform unrealistically for the salinity and the temperature outside the measurement range. Again, P and Q in the expression need to be kept as small as possible to mitigate the errors when extrapolating outside the measurement range.

APPENDIX C

SUMMARY OF GW2020 MODEL FUNCTION

This appendix summaries the expressions of the GW2020 model function for the convenience of readers. The representation of all the parameters have been mentioned in the paper, which will not be repeated in the appendix.

The GW2020 model function is given by:

$$\varepsilon_{sw}(S,T) = \varepsilon_{\infty} + \frac{\varepsilon_{s-dw}(T)R_{sw-dw}(S,T) - \varepsilon_{\infty}}{1 + j\omega\tau(T)} - \frac{j\sigma(S,T)}{\omega\varepsilon_0}$$

where,

S: salinity in psu, T: temperature in degree Celcius (°C),

$\varepsilon_{\infty} = 4.9$, $\varepsilon_0 = 8.8542\text{E}-12$,

$$\tau(T) = 1.75030\text{E-}11 - 6.12993\text{E-}13 \cdot T + 1.24504\text{E-}14 \cdot T^2 - 1.14927\text{E-}16 \cdot T^3,$$

$$\varepsilon_{s-dw}(T) = 8.80516\text{E+}01 - 4.01796\text{E-}01 \cdot T - 5.10271\text{E-}05 \cdot T^2 + 2.55892\text{E-}05 \cdot T^3,$$

$$R_{sw-dw}(S,T) = 1 - S \cdot (3.97185\text{E-}03 - 2.49205\text{E-}05 \cdot T - 4.27558\text{E-}05 \cdot S + 3.92825\text{E-}07 \cdot ST + 4.15350\text{E-}07 \cdot S^2),$$

$$\sigma(S,T) = (9.50470\text{E-}02 \cdot S - 4.30858\text{E-}04 \cdot S^2 + 2.16182\text{E-}06 \cdot S^3) \cdot [1 + T \cdot (3.76017\text{E-}02 + 6.32830\text{E-}05 \cdot T + 4.83420\text{E-}07 \cdot T^2 - 3.97484\text{E-}04 \cdot S + 6.26522\text{E-}06 \cdot S^2)].$$

ACKNOWLEDGMENTS

The first two authors would like to thank the Physical Oceanography Program at the National Aeronautics and Space Administration (NASA) for their financial support under grants: NN17AK01G and NNG05GO48G for this work. Dr. Dinnat's work was supported by NASA, grant 80NSSC18K1443. We gratefully thank the help from Mr. Duncan d'Hemecourt and Mr. Young Soung Park for optimizing the control system of the seawater dielectric experiment.

REFERENCES

[1] Y. H. Kerr et al., "The SMOS Mission: New Tool for Monitoring Key Elements of the Global Water Cycle", *Proc. IEEE*, vol. 98, no.5, pp. 666–687, Apr. 2010

[2] G. Lagerloef, F. R. Colomb, D. Le Vine, F. Wentz, S. Yueh, C. Ruf, J. Lilly, J. Gunn, Y. Chao, A. deCharon, G. Feldman and C. Swift, "The Aquarius/SAC-D mission – Designed to Meet the Salinity Remote Sensing Challenge", *Oceanography*, vol. 21, no.1, pp. 68-81, Mar. 2008

[3] D. M. Le Vine, G. Lagerloef and S.E. Torrusio, "Aquarius and Remote Sensing of Sea Surface Salinity from Space", *Proc. IEEE,* vol. 98, no. 5, pp. 688-703, Apr. 2010

[4] D. Entekhabi, E. G. Njoku, P. E. O'Neill, K. H. Kellogg et al., "The Soil Moisture Active Passive (SMAP) Mission", *Proc. IEEE*, vol. 98, no. 5, pp. 704-716, May 2010

[5] E. Dinnat, J. Boutin, G. Caudal, J. Etcheto and P. Waldteufel, "Influence of Sea Surface Emissivity Model Parameters at L-band for the Estimation of Salinity", *Int. J. Remote Sens.*, vol. 23, no. 23, pp. 5117-5122, Nov. 2010

[6] A. Stogryn, H. T. Bull, K. Rubayi and S. Iravanchy, "The microwave permittivity of sea and fresh water", *Tech. Rep., Gen. Crop Aerojet*, Azusa, CA, 1995

[7] W. A. Ho and W. F. Hall, "Measurements of the dielectric properties of seawater and NaCl solutions at 2.65 GHz" *Journal of Geophysical Research*, vol.78, pp. 6301-6315, Sep. 1973

[8] W. A. Ho, W. Love and M. J. Van Melle, "Measurements of the dielectric properties of sea water at 1.43 GHz" *NASA Contract Rep*. CR-2458, Dec. 1974

[9] M. D. Blue, "Permittivity of ice and water at millimeter wavelengths", *Journal of Geophysical Research*, vol.85, no. C2, pp.1101-1106, Feb. 1980

[10] W. Ellison, A. Balana, G. Delbos, K. Lamkaouchi et al., "New permittivity measurements of seawater", *Radio Sci.*, vol. 33 pp. 639-648, May 1998

[11] S. Blanch and A. Aguasca, "Seawater dielectric permittivity model from measurements at L band", *Proceedings of IGARSS*, pp.1362-1365, Sep. 2004

[12] R. Lang, Y. Zhou, C. Utku, and D. Le Vine, "Accurate measurements of the dielectric constant of seawater at L band", *Radio Sci.*, vol.51, pp. 2-24, Jan. 2016

[13] A. Stogryn, "Equations for calculating the dielectric constant of saline water", *IEEE Trans. Microwave Theory Tech*., vol. 19, no.8, pp. 733-736, Aug. 1971

[14] L. Klein and C. Swift, "An improved model for the dielectric constant of sea water at microwave frequencies", *IEEE J. Oceanic Eng.*, vol. 25, no.1, pp. 104-111, Jan. 1977

[15] T. Meissner and F. Wentz, "The complex dielectric constant of pure and sea water from microwave satellite observations", *IEEE Trans. Geosci. Remote Sens.*, vol.42, no. 9, pp.1836-1849, Sep. 2004

[16] T. Meissner and F. Wentz, "The emissivity of the ocean surface between 6 and 90 GHz over a large range of wind speeds and earth incident angles", *IEEE Trans. Geosci. Remote Sens.*, vol. 50, no. 8, pp. 3004-3026, Aug. 2012

[17] T. Meissner, F. J. Wentz, and L. Ricciardulli, "The emission and scattering of L-band microwave radiation from rough ocean surfaces and wind speed measurements from the Aquarius sensor", *J. Geophys. Res. Ocean.*, vol. 119, no.9, pp. 6499–6522, Sep. 2014

[18] Y. Zhou, R. Lang, E. Dinnat and D. Le Vine, "L-band model function of the dielectric constant of seawater", *Trans. Geosci. Remote Sens.*, vol. 55, no.12, pp. 6964-6974, Dec. 2017

[19] E. Dinnat, D. Le Vine, J. Boutin, T. Meissner, and G. Lagerloef, "Remote Sensing of Sea Surface Salinity: Comparison of Satellite and In Situ Observations and Impact of Retrieval Parameters", *Remote Sensing*, vol. 11, no.7, 750, Mar. 2019 https://doi.org/10.3390/rs11070750

[20] Y. Zhou, R. Lang, E. Dinnat and D. Le Vine, "Seawater dielectric measurements at L-band with latest improvements", *IGARSS*, Valencia, Spain, Jul. 2018, doi: 10.1109/IGARSS.2018. 8517277

[21] E. Olmedo, C. Gabarró, V. González-Gambau , J. Martínez, "Seven Years of SMOS Sea Surface Salinity at High Latitudes: Variability in Arctic and Sub-Arctic Regions", *Remote Sens.,* vol. 10, no.11, 1772, Nov. 2018

[22] S. Yueh, R. West, W. Wilson, F. Li, S. Nghiem, Y. Rahmat-Samii, "Error Sources and Feasibility for Microwave Remote Sensing of Ocean Surface Salinity". *IEEE Trans. Geosci. Remote Sens.*, vol. 39, no.5, pp.1049–1059, May 2001

[23] Z. Liu, K. Muldrew, R.G. Wan, J. A. Elliott, "Measurement of freezing point depression of water in glass capillaries and the associated ice front shape", *Phys. Rev. E*, vol. 67, no.6, 061602, Jun. 2003

[24] U. Kaatze, "Complex Permittivity of Pure Water as a Function of Frequency and Temperature", *J. Chem. Eng. Data*, vol.34, no.4, pp. 371-374, Oct. 1989

[25] R. Somaraju and J. Trumpf, "Frequency, Temperature and Salinity Variation of the Permittivity of Seawater", IEEE *Trans. Antennas Propag.*, vol. 54, no. 11, Nov. 2006

[26] E. P. Dinnat and D. M. Le Vine, "Effects of the Antenna Aperture on Remote Sensing of Sea Surface Salinity at L-Band," *IEEE Trans. Geosci. Remote Sens.*, vol. 45, no. 7, pp. 2051–2060, Jul. 2007.

[27] T. Meissner, F. J. Wentz, and D. M. Le Vine, "The salinity retrieval algorithms for the NASA Aquarius version 5 and SMAP version 3 releases," *Remote Sens.*, vol. 10, no. 7, Jul. 2018.

[28] T. Meissner, F. Wentz, D. Le Vine, "Aquarius Salinity Retrieval Algorithm Theoretical Basis Document (ATBD), End of Mission Version", RSS Technical Report 120117. Dec. 2017. Available at: http://dx.doi.org/10.5067/DOCUM-AQR04. (accessed on 10 July 2018)

[29] S. C. Riser, H. J. Freeland, Roemmich.et al., "Fifteen years of ocean observations with the global Argo array. Nature Clim. Change", vol. 6 , pp. 145–153, Jan. 2016, Available at: https://doi.org/10.1038/nclimate2872

[30] S. Misra and C. Ruf, "Detection of Radio-Frequency Interference for the Aquarius Radiometer", IEEE Trans Geosci. Remote Sens., vol. 46, no.10, pp. 3123-3128, Oct. 2008